Environmental Science and Pollution Research (2023) 30:12169–12188
https://doi.org/10.1007/s11356-022-22848-6

RESEARCH ARTICLE

Experimental investigation of thermal efficiency and thermal performance improvement of compound parabolic collector utilizing SiO_2/Ethylene glycol–water nanofluid

Omid Khaledi[1] · Seyfolah Saedodin[1] · Seyed Hadi Rostamian[2]

Received: 13 June 2022 / Accepted: 29 August 2022 / Published online: 15 September 2022

Abstract

A compound parabolic collector has been used in the present study to lower operating costs per unit of heat increase compared to other tracker concentrators. This type of collector has been given more attention in industrial and domestic applications in the temperature range of 60 to 300 °C. Also, to increase the thermal efficiency, nanofluid containing SiO_2 nanoparticles in ethylene glycol–water hybrid base fluid (10–90 vol.%) have been used in three different volumetric fractions. The innovation of this present study includes the utilization of mentioned nanofluids for the first time in this collector, which has good stability and is cost-effective compared to other nanoparticles. In addition, the experimental measurement of thermal and hydraulic properties of nanofluids represents new aspects of the present study. The experiments used three volumetric fractions of 0.5%, 1%, and 1.5% under extensive solar radiation. Thermal performance of the collector at four volumetric flow rates of 1, 1.5, 2, and 2.5 Lit/min have been investigated according to ASHRAE standard 93–2010 (RA2014). According to the experimental data, the thermal efficiency of the collector improved by 5% to 11.6% when the nanofluid was applied. The maximum enhancement of the average Nusselt number of the nanofluid versus the base fluid at the volumetric flow rate of 1 Lit/min and the volumetric fraction of 1.5% was equal to 7.3%. Besides, nanofluid increased the pressure drop, and consequently, the pumping power slightly. Finally, considering both the impacts of heat transfer and pressure drop, performance evaluation criteria and overall efficiency for nanofluid have been analyzed. The results represented that in all volumetric fractions, the values of performance evaluation criteria and overall efficiency enhanced compared to the base fluid. This research provides researchers and engineers with important information to better understand the thermal and hydraulic parameters of the parabolic compound concentrator in the presence of nanofluid to improve its thermal performance. The results also highlight the potential of using SiO_2 nanoparticles to improve the thermal efficiency of solar collectors despite their low thermal conductivity compared to other conventional nanoparticles.

Keywords Compound parabolic collector (CPC) · Nanofluid containing silica · Heat transfer · Thermal efficiency · Experimental investigation

Nomenclature

A_a	The CPC collector aperture area $\left(m^2\right)$
A_r	The absorber tube area $\left(m^2\right)$
C	Concentration ratio
C_p	Specific heat of the heat transfer fluid $(j/kg.K)$
f	Friction factor
F_R	Heat removal factor
H	Height of CPC collector (m)
h	Heat transfer coefficient $(W/m^2.K)$
I_{eff}	Efficient solar irradiation (W/m^2)
k	Thermal conductivity $(W/m.K)$
$\dot{m}$	Mass flow rate (kg/s)
$\overline{Nu}$	Average Nusselt number
$\dot{Q}_s$	Total solar radiation rate (W)
$\dot{Q}_u$	Net useful heat gain rate (W)
r	Radius (m)
Re	Reynolds number
T	Temperature (K)
T_{Amb}	Ambient temperature (K)
T_{fave}	Average temperature of the fluid (K)

Responsible editor: Philippe Garrigues

✉ Seyed Hadi Rostamian
h.rostamian@du.ac.ir

Omid Khaledi
omid.khaledi@semnan.ac.ir

[1] Faculty of Mechanical Engineering, Semnan University, Semnan, Iran

[2] School of Engineering, Damghan University, Damghan, Iran

T_r	Reduced Temperature ($°Cm^2/W$)
T_s	Mean temperature of the absorber surface (K)
U_C	Uncertainty
U_L	Heat loss coefficient ($W/°Cm^2$)
u_m	Average fluid velocity (m/s)
$\dot{V}$	Volumetric flow rate (Lit/min)
W	Width of the CPC collector (m)
$\dot{W}_p$	Pumping power (W)

Greek Symbols

ΔP	Pressure drop (pa)
η_{el}	Electrical efficiency
η_0	Maximum optical efficiency
η_{ovr}	Overall efficiency
η_{th}	Thermal efficiency
θ	Incident angle (°)
μ	Dynamic viscosity ($Pa.s$)
ρ	Density (Kg/m^3)
ϕ	Volumetric fraction
μ	Dynamic viscosity ($Pa.s$)

Subscripts

ai	Inner surfaces of the absorbent tube
ao	Outer surfaces of the absorbent tube
bf	Base fluid
Exp	Experimental
f	Fluid
fi	Inlet heat transfer fluid
fo	Outlet heat transfer fluid
nf	Nanofluid
np	Nanoparticle

Abbreviation

CPC	Compound parabolic concentrator
CTC	Cylindrical trough collector
EG	Ethylene glycol
ETC	Evacuated tube collector
FPC	Flat-plate collector
HFC	Heliostat field collector
HTF	Heat transfer fluid
LFR	Linear Fresnel reflector
NF	Nanofluid
NP	Nanoparticle
PDR	Parabolic dish reflector
PEC	Performance evaluation criterion
PTC	Parabolic trough collector
SHC	Specific heat capacity
TE	Thermal efficiency
TP	Thermal performance
VRF	Volumetric flow rate

Introduction

An increase in demand for energy, the reduction in consumption of fossil fuel environmental considerations, and the increasing cost of their use deems necessary to develop new energy-saving methods (Dadashi et al. 2022; Unar et al. 2021). In addition, the consumption of fossil fuels increases the concentration of greenhouse gases and global warming. Solar energy is one of the renewable energy sources available to humans that has received significant attention. In this regard, solar energy can fulfill the need of countries (Esfanjani et al. 2022).

Due to the broad range of acceptance angles and non-sun-tracking configurations, non-imaging collectors are used in home and industrial applications in the temperature range of 60 to 300 °C. In particular, research and development on CPC collectors have been extensive since the 1980s, but studies on CPC collectors with tubular receptors are more limited, although it possesses a high potential in industrial and domestic applications at low and medium temperatures (Brunold et al. 1994; Fernández-García et al. 2010; Naveenkumar et al. 2021). However, interest in using collectors with low and medium temperatures has recently increased (Panahi et al. 2019). Table 1 displays the position of CPC

Table 1 Different types of solar collector in thermal usage (Kalogirou 2014)

Motion	Collector type	Concentration ratio	Absorber type	Indicative temperature range (°C)
Stationary	FPC	1	Flat	30–80
	ETC	1	Flat	50–200
	CPC	1–5	Tubular	60–240
Single-axis tracking	CPC	5–15	Tubular	60–300
	LFR	10–40	Tubular	60–250
	CTC	15–50	Tubular	60–300
	PTC	10–85	Tubular	60–400
Two-axis tracking	PDR	600–2000	Point	100–1500
	HFC	300–1500	Point	150–2000

collectors among various types of collectors (Kalogirou 2014; Ustaoglu et al. 2016).

Improving the efficiency of solar collectors using various methods provides the basis for more use of solar energy. To improve the TE of solar collectors, many researchers have proposed ways to enhance the heat transfer rate between the absorber and the HTF whereas enhanced heat transfer properties of HTF are a preferred approach. For example, NFs, which are NP suspensions (less than 100 nm in size), can be added to HTF to increase their thermal properties and, consequently, the TE of the collector. In recent years, NFs have been promising in various heat transfer applications, particularly in solar collectors, due to their enhanced thermal conductivity compared to pure fluids (Bellos et al. 2020; Izadi et al. 2013; Sajjadi 2021; Shafiey Dehaj et al. 2020; Yan et al. 2020). Most recent studies have reported significant enhancements in the thermal and optical performance of solar collectors operating on NFs. The TE showed proportionally dependent on the concentration of NPs in regular fluids with reasonable values (Izadi et al. 2014; Shehzad et al. 2021; Xiong et al. 2021a, 2021b). It should be noted that many studies have examined NF-based solar collectors experimentally and numerically so far. Ezadi and Haj Asaad (Izadi & El Haj Assad 2021) investigated the use of NF in solar energy systems in detailed research. They explored different types of collectors as well as one of the most important passive methods in increasing the efficiency of solar energy absorption, namely the use of NFs as the working fluid. In a review article, Xiong et al. (Xiong et al. 2021a, 2021b) provide an overview of the distinct types of particles used in NF research with an emphasis on their application in solar collectors. In this review, works concerning the application of NFs in solar collectors are singled out and analyzed. They concluded that non-metallic NP-based NFs could be more beneficial for the efficiency enhancement of solar collectors compared to metal NP-based NFs.

The application of NFs containing silica has been considered by many researchers due to its cost-efficient and good stability suspension of NPs (Khaledi et al. 2022a, b; Kharabati et al. 2021; Rostamian et al. 2022). Javanian et al. (Jouybari et al. 2017) studied the TP of deionized water-SiO_2 with volumetric fractions of 0.2%, 0.4%, and 0.6% in an FPC with a porous metal channel, and they showed that the TE improves by 8.1%. Their results showed that raising the volumetric fraction of NPs from 0.2 to 0.6%, the PECnf increases at VFR of 0.5 Lit/min from 1.07 to 1.34. In addition, Sharafeldin et al. (Sharafeldin and Gróf 2018) studied SiO_2-water NFs in a collector with direct adsorption in evacuated tubes. The researchers came to this conclusion that due to agglomeration problems at higher concentrations, the proper concentration was 1%. The impact of SiO_2 dispersed in EG-water on TP of FPC was studied by Salavati et al. (Salavati Meibodi et al. 2015). Their outcomes highlight the extraordinary ability NPs of SiO_2 despite its lower thermal conductivity than oxide NPs in increasing the TP of FPC. In experimental research, Farhana et al. (Farhana et al. 2021) studied the effect of crystal nano-cellulose NFs (CNC) on the TE of FPC. They first measured the thermophysical properties of two NFs, Al_2O_3/EG-water, and CNC/EG-water, and then showed the energy gain, HTF outlet temperature, and TE of the FPC when using the NF. Okonkwo et al. (Okonkwo et al. 2020) developed a numerical thermal model to evaluate the performance of an FPC based on Al_2O_3/water NF and Fe-Al_2O_3/water hybrid NF to investigate the first and second rules of thermodynamics. Their results represented that the use of Al_2O_3/water at a volumetric fraction of 0.1% showed a 2.16% increase in heat in the collector, while hybrid NFs reduced the TP of the collector by 1.79% compared to water. They showed that although the usage of hybrid NFs does not provide a superior thermal choice for water, but exergy efficiency increases when using hybrid NFs and mono NFs.

The utilization of NFs in solar concentrator technology has been studied extensively in multitude concentrators (Rashidi et al. 2021; Sadeghi et al. 2020; Tahani et al. 2016; Xiong et al. 2021a, b). Most studies in this field were for PTCs, and there is sufficient research on ETC with reflectors and concentrating photovoltaic thermal (Akbarzadeh and Valipour 2018; Mahian et al. 2013). Limited studies examined use of NFs in CPC collectors to increase TP. Khaledi et al. (Khaledi et al. 2022b) experimentally investigated the thermal performance and exergy analysis of a MWCNT-SiO_2 (10–90%)/EG-water (10–90 vol.%) hybrid NF in a CPC collector. The results of extensive experiments showed that use of hybrid NF leads to an increase in TE compared to the base fluid due to the improvement of thermal properties and Nusselt number. At a VFR of 2.5 Lit/min and a volumetric fraction of 1.5%, they reported an enhancement in TE and exergy efficiency compared to the base fluid by 14.27% and 45%, respectively. The test results represented that the maximum increase in pumping power using hybrid NF is 9.72%, which increases the demand for pumping power is very small compared to the net production of usable heat rate. Kors et al. (Korres et al. 2019) researched the TE of a CPC collector with a working fluid of Syltherm 800– CuO in a numerical simulation. Results for a volumetric fraction of 5% and an inlet temperature of 25 to 300 °C, the average increment in TE occurs at 1.24%, and the maximum enhancement of TE is 2.76%. The average and maximum increments in heat transfer coefficient have respectively been 16.16 and 17.41%. It also was found that using NFs, the maximum increase in TE is 2.60%, and the overall efficiency increment is up to 2.76%. The result of their study was the use of NFs in the CPC collector, which enhances the TE alongside a slight pressure drop. Sadeghizad et al. (Sadeghiazad and Yahou 2018) studied the heat transfer process in a

CPC collector with two hot and cold return tubes utilizing Al_2O_3 NPs in water as the working fluid. Their numerical analysis performed using the finite volume method under steady-state conditions; they investigated the impacts of time on heat transfer inside the tubes during a day. Their results illustrated that with the highest temperature differences between the inlet and outlet of the CPC collector tubes, maximum heat transfer occurs at noon. Mahboub et al. (Mahbubul et al. 2018) evaluated a CPC collector using a discharged water-SWCNT tube as HTF. Their results showed a 66% increase in TE when using NF with a volumetric fraction of 0.2%. Lee et al. (Li et al. 2015a, 2015b) tested the impacts of water-MWCNTs as NFs on the performance of a CPC collector with an internal tracking mechanism with two various absorbers tube of a black chrome-plated copper tube and a glass tube. The outcomes represented that the highest TE of the collector for the absorber tube with black cream coating and glass tube was 73% and 85%, respectively. They concluded the reason for such behavior could be more reflection and a drop in emission from the glass surface.

According to the previous studies, most researches have presented the effects of various working NFs on different collectors. Based on the latest review, there was no research done to determine the effect of SiO_2/EG-water NF on the thermal and hydraulic performance of CPC collectors, although Salavati Meibodi et al. (Salavati Meibodi et al. 2015) found that SiO_2/EG-water NF had good thermal properties. On the other hand, SiO_2 NPs have some advantages such as easy preparation process, low price, high hydrophilic properties, high stability of it with EG-water compared to other NPs, no toxicity or flammability when it was using and environmentally friendly, that increase its economic potential and commercialization.

It is worth mentioning that for the first time after making a stable SiO_2/EG-water NF using an ultrasonic technique, the thermophysical and hydraulic properties of SiO_2/EG-water NF have been measured and calculated at different concentrations and temperatures. Besides, examining what extent thermal and hydraulic performance of CPC collectors is affected by adding SiO_2 NPs, different concentrations and using various VFRs are deeply investigated in this paper. A detailed discussion about the effect of environmental parameters like ambient temperature and wide range of solar radiation spectrum included in the presented work by using the reduced temperature parameter as the independent variable in several figures. Also, to simultaneously determine the effects of NF on heat transfer rate, the adverse effect of increasing the HTF friction factor (pressure drop) and increasing the pumping power evaluated by the appropriate criteria of PEC and overall efficiency.

Materials and methodology

In this section, the procedure used to prepare the SiO_2/EG-water NF mixtures is discussed. In addition, the experimental setup is presented. The technical specifications of the CPC collector are presented and the geographical location and details of the tests site are specified. Then, experimental procedure and governing equations descripted.

Preparation of SiO_2/EG–water (10:90 vol.%) NFs

In order to produce NFs, NPs of SiO_2 with a medium size of 20–30 nm were dispersed in EG-water (10–90%) based fluid. The main thermo-physical properties of SiO_2, deionized water and EG are given in Table 2. The NF are prepared in volumetric fractions of 0.5%, 1%, and 1.5%. The suspension is stirred by a magnetic stirrer for 2 h at this stage. Afterwards it is placed inside an ultrasonic homogenizer with a power of 400 W and 20 kHz in order to decompose the aggregation between the NPs and minimize the scale. After every 10 min of sonication, the suspension is stirred with a stirrer for 20 min. This process is repeated alternately to achieve the desired stability. Ultrasonic waves duration varies depending on the volumetric fraction. Figure 1 shows the SiO_2 NPs and prepared NF after 1 month. As can be seen, no sedimentation was beheld with the naked eye during this period. It should be noted that due to the hydrophilicity of silica NPs, no surfactant was used in the suspension process of this NF.

The images of SEM and XRD analysis of SiO_2 NPs are displayed in Fig. 2. The images of scanning electron microscope are one of the most current and well-known methods for studying the size of NPs that are often used by various researchers. In addition, XRD analysis is used to analyze

Table 2 Thermo-physical and textural properties of SiO_2 NP and base fluids (Minea 2017; Salavati Meibodi et al. 2015)

Substance	Color	Purity	Density (kg/m^3)	Specific surface area (m^2/g)	Pore size (nm)	Thermal conductivity ($W/m.K$)	Specific heat capacity ($J/kg.K$)
SiO_2	white	99.5%	2200	200	24.58	1.4	703
Deionized water	-	-	996	-	-	0.613	4180
EG	-	-	1115	-	-	0.253	2415

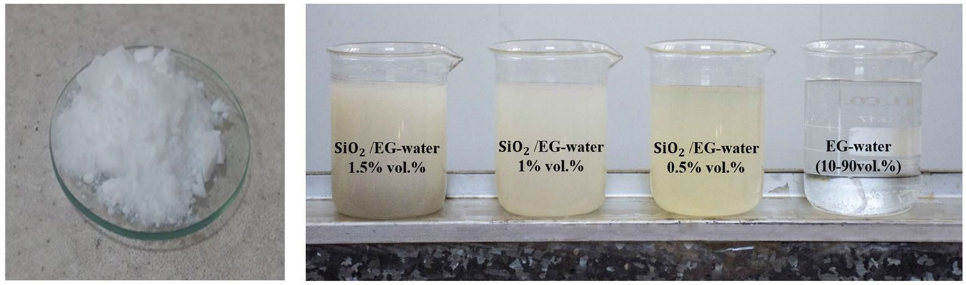

(a) (b)

Fig. 1 (**a**) NPs SiO_2 belong to AROSIL @ 200, (**b**) The prepared base fluid and NFs after one months

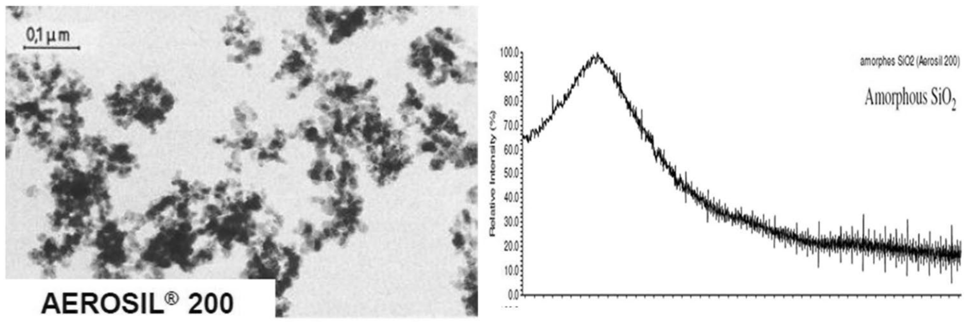

(a) (b)

Fig. 2 (**a**) SEM photo of SiO_2 NPs, (**b**) XRD photo of SiO_2 NP

the material, the purity and the crystal size of the NPs used in this study.

Experimental setup

The schematic of experimental set-up and its measuring equipment are presented in Fig. 3. Overall, the set-up includes measuring equipment, fluid circulation equipment and a test section. In the present study, the test section is a CPC collector. This set-up is located in the Science and Technology Park of Semnan University in Iran. This city, Semnan, is in *latitude* $35^{\circ}14'3.00''N$ and *longitude* $53^{\circ}55'8.99''E$, at an altitude of 1350 m above sea level. The designed CPC collector is located on a movable and adjustable structure. The CPC collector's main axis is located in the west–east direction and to the south with a slope angle of 45. The amount of solar flux measured varied from $650W/m^2$ to $1100W/m^2$. A Grundfos-UPS series pump was installed at the outlet of the supply tank to circulate the HTF in a closed cycle inside the absorber tube and the solar system. According to ASHRAE standard 93–2010 (RA2014) (Ashrae 2014), a heat exchanger was used inside the closed cycle to control the inlet temperature to the test section. Two PT100-type RTD sensors have been used in the test section to detect the inlet temperature and the outlet temperature of the HTF. Also, the surface temperature of the absorber tube was evaluated by five thermocouple-type K. The accuracy of PT100 sensors and thermocouples-type K is equal to ± 0.1 °C. The VFR was calculated by a flowmeter with an uncertainty ±2%. A bypass line in the cycle has been used to the flow airtightness as well as to regulate and control the VFR. A solar power meter TES-1333R with an uncertainty of ±2.5% was used to determine the radiant heat flux. Two pressure transmitters were utilized at the outlet and inlet of the absorber tube to estimate the pressure drop of the HTF with an uncertainty of less than ±0.1%. An AcoLab-LX8 data logger server, Aco 240L temperature data logger, Aco 724L current data logger and Aco-400P portal weight data logger manufactured by Aco Afra Company (shown in Fig. 4) was used to record various system variables and store test data. The inlet temperature and outlet temperature of the HTF, absorber tube surface temperature, ambient temperature, solar radiation at the CPC collector aperture area, VFR, pressure drop and wind speed were the experimental variables recorded in this test. Table 3 and Fig. 5 display the technical specifications of the CPC collector and schematic of the coaxial tubular the CPC collector of the present investigation, respectively.

Experimental procedure

The TP characteristics of the CPC collector are settled in accordance with ASHRAE standard 93–2010 (RA2014). To determine TE according to the ASHRAE standard, it is necessary to maintain stable conditions during the test period and for a restricted time before the test which is called pre-data period. Consistent with ASHRAE standard, this parameter is 15 min, and the data measurement interval is

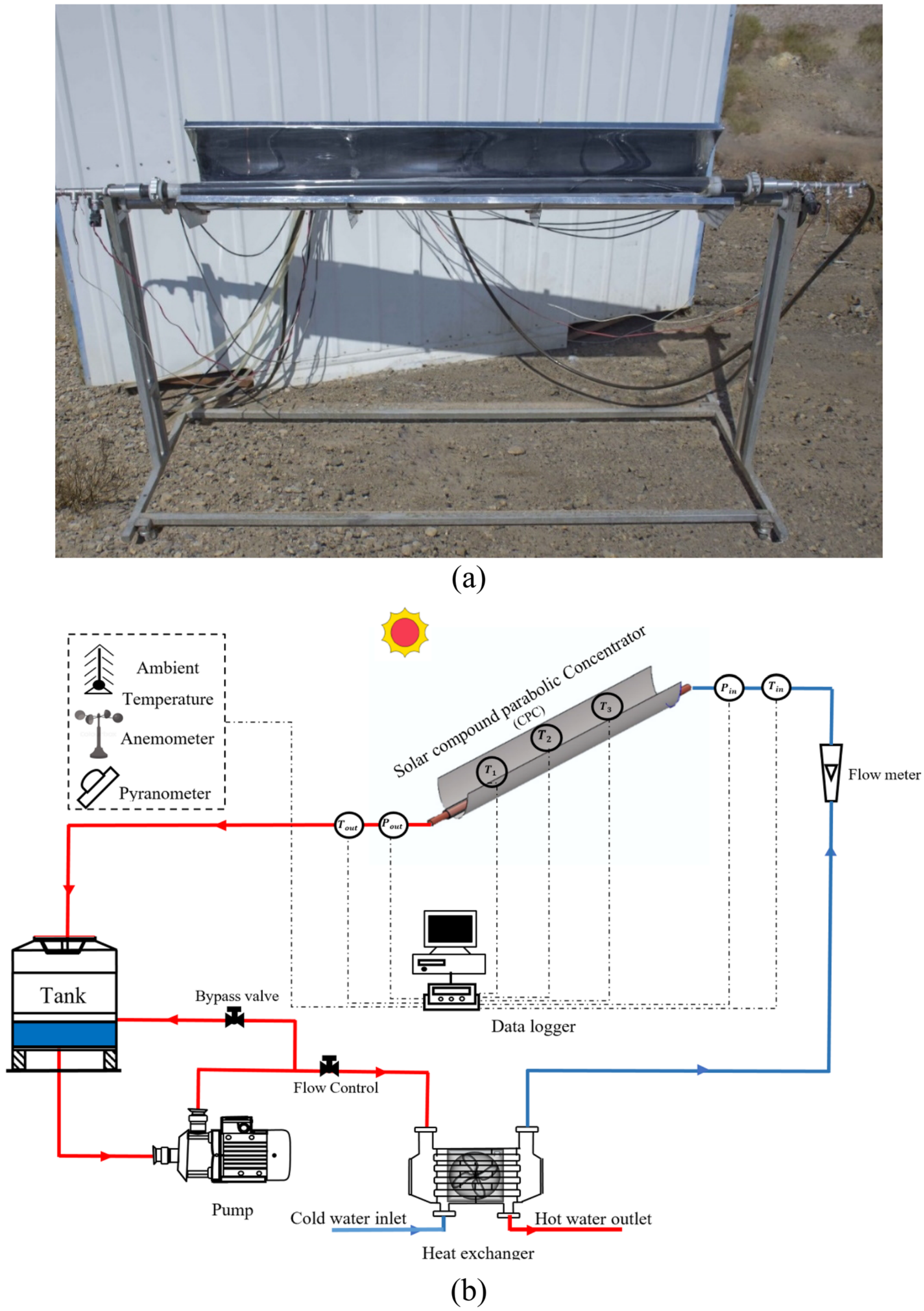

Fig. 3 (**a**) The CPC collector test equipment, and (**b**) Schematic diagram of the hydraulic cycle

5 min in this research. The measured data is also symmetrical with the solar noon, which reduces the number of experiment days. It is important to consider that climate change on test days may violate the requirements of the ASHRAE standard and impact the measurement of data. To ensure the replicability of the tests and gain a satisfactory accuracy, each test was duplicated three times. The acceptable variations of variables and environmental conditions that must be achieved to utilization the ASHRAE standard 93–2010 (RA2014) are listed in Table 4.

Governing equations

Thermal performance analysis of the CPC collector

By measurement, the inlet and outlet temperature of the HTF, the net rate of useful heat gain of the HTF could be calculated using Eq. (1) (Duffie et al. 1985).

$$\dot{Q}_u = \dot{m}C_p\left(T_{fo} - T_{fi}\right) = \rho_f \dot{V} C_p\left(T_{fo} - T_{fi}\right) \tag{1}$$

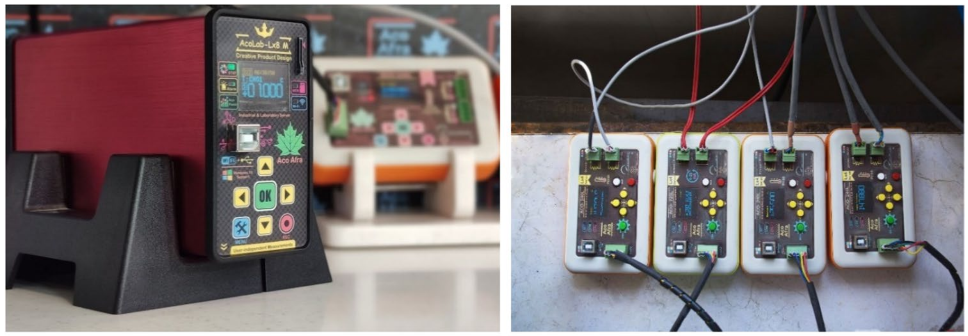

(a) (b)

Fig. 4 (**a**) AcoLab-Lx8 Data logger server, and (**b**) Different temperatures and current data logger modules for measuring CPC collector variables

Table 3 The materials and technical specifications of the CPC collector

	Parameters	Symbols	Dimension
CPC	Aperture area	A_a	0.3795 m^2
	Acceptance angle	θ_C	35°
	Collector length	L	1.65 m
	Collector height	H_{cpc}	0.23 m
	Collector width	W_{cpc}	0.23 m
	concentration ratio	C	1.7
	optical efficiency	η_0	0.67
Glass envelope	Outer diameter	D_{g_o}	59 mm
	Inner diameter	$D_{g_{oi}}$	54 mm
	Transmittance	τ_g	0.97
	Emittance	ε_g	0.88
Copper absorber tube (Selective absorption coating)	Outer diameter	D_{a_o}	42 mm
	Inner diameter	D_{a_i}	38.2 mm
	Conductivity	k_a	$400W/mK$
	Absorptivity	α_a	0.93
	Emittance	ε_a	0.13

The net rate of useful heat gain of the HTF could be stated according to the values of the absorbed energy parameter, $F_R\eta_0$ and the removed energy parameter, F_RU_L (Duffie et al. 1985).

$$\dot{Q}_u = F_R\left[A_aI_{eff}\eta_0 - A_rU_L\left(T_{fi} - T_{Amb}\right)\right] \tag{2}$$

The TE of the CPC collector is a measure of its TP and is explained as the ratio of the net rate of useful heat gain of the HTF to the efficient solar irradiation of the incidence on the CPC collector aperture area (Duffie et al. 1985).

$$\eta_{th} = \frac{\dot{Q}_u}{A_aI_{eff}} = \frac{\dot{m}C_p\left(T_{fo} - T_{fi}\right)}{A_aI_{eff}} \tag{3}$$

By replacing the useful energy of Eq. (2) in Eq. (3), the TE in steady state condition is obtained as follows (Duffie et al. 1985).

$$\eta_{th} = F_R\eta_0 - \frac{F_RU_L}{C}\frac{\left(T_{fi} - T_{Amb}\right)}{I_{eff}} \tag{4}$$

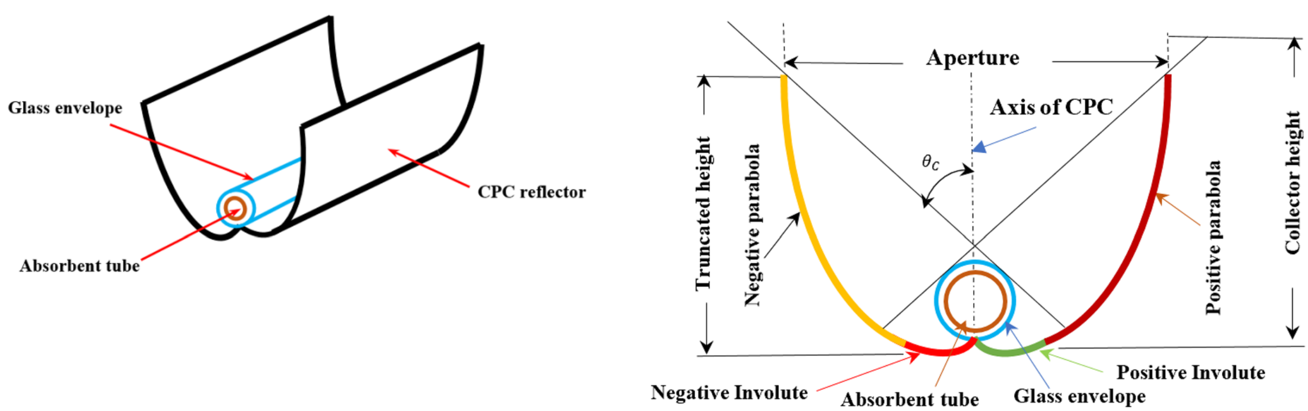

(a) (b)

Fig. 5 (**a**) 3D schematic of the CPC collector, and (**b**) 2D Schematic of the coaxial tubular CPC collector

Table 4 Requirements for environmental conditions and allowable values of parameter variations according to ASHRAE standard (ASHRAE 2014)

Parameters	Ranges	Maximum variations
Solar heat flux	$> 800W/m^2$	± 32
The fraction of diffusion	$20\ \%\ (maximum)$	-
Wind velocity	$2m/s < u < 4m/s$	-
Environmental temperature	-	$\pm 1.5K$
The rate of flow	-	$\pm 2\ \%\ or \pm 0.005\ gpm,\ which\ is\ greater$
Inlet temperature	-	$\pm 2\ \%\ or\ 1K,\ which\ is\ greater$

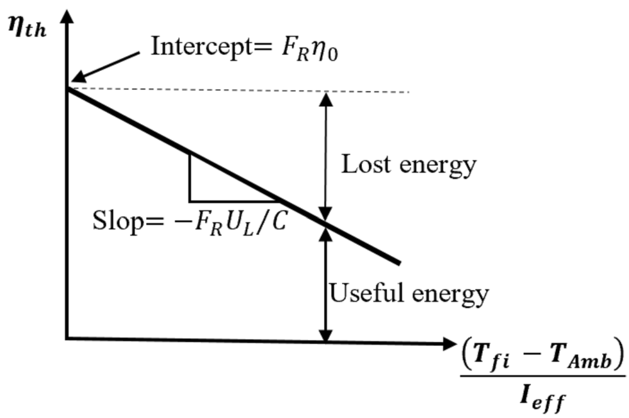

Fig. 6 Schematic diagram of the thermal efficiency curve (Duffie et al. 1985)

TE tests are performed around noon solar, in conditions close to normal incidence irradiation. In this case, the values of η_0, F_R و and U_L do not change much in the range of conditions of the test. TE could be plotted against the amount of reduced temperature, $\left(T_{fi} - T_{Amb}\right)/I_{eff}$, which will be obtained as a straight line. The crossing of this line with the vertical axis represented the $F_R\eta_0$ and the slope of the line displays the $F_R U_L/C$ from the CPC collector (Duffie et al. 1985). A schematic diagram of TE is presented in Fig. 6.

Convective heat transfer is the main mechanism of heat transfer between the absorber tube and the HTF. The Nu is therefore utilized as a dimensionless parameter to define heat transfer The value of heat transfer coefficient could be shown as (Bejan 2004).

$$h = \frac{\dot{Q}_u}{2\pi r_{a_o} L\left(T_s - \frac{T_{fi}+T_{fo}}{2}\right)} \tag{5}$$

According to the definition of heat transfer concepts, the $\overline{Nu}$ between the absorber tube and the HTF is calculated according to Eq. (6) (Bejan 2004).

$$\overline{Nu} = \frac{2hr_{a_i}}{k_f} \tag{6}$$

Also, the Reynolds number is explained as follows.

$$Re = \frac{2\rho_f \dot{V}}{\pi r_{a_i} \mu} \tag{7}$$

Hydraulic analysis of the CPC collector

To calculate the pressure drop in the CPC collector, pressure sensors installed at the inlet and outlet of the absorber tube are being used. By having the pressure drop, the friction factor and the demanded pumping power could be calculated. The value of the empirical friction factor is estimated according to Eq. (8) (Çengel and Cimbala 2013).

$$f_{Exp} = \frac{\Delta P_{Exp}}{\frac{L}{2r_{a_i}}\left(\frac{1}{2}\rho_f u_m^2\right)} \tag{8}$$

where u_m is the average velocity of the HTF in the absorber tube and is calculated from Eq. (9) (Çengel and Cimbala 2013).

$$u_m = \frac{\dot{m}}{\rho_f \pi r_{a_i}^2} \tag{9}$$

The demanded pumping power to circulate HTF in the closed cycle is estimated using Eq. (10) (Çengel and Cimbala 2013).

$$\dot{W}_p = \frac{\dot{m}\Delta P}{\rho_f} = \dot{V}\Delta P \tag{10}$$

Evaluation indexes of the CPC collector

The PEC and the overall efficiency of the CPC collector are being employed to simultaneously evaluate the increasement of heat and the rise of pressure drop. In general, the outcomes obtained from NFs are apparently attractive regarding thermal properties. Nevertheless, one crucial point needs to be disputed. In fact, increasing the dynamic viscosity of NFs certainly involves the increasement of pressure drop within the system, followed by enhancing the work of the associated pump. As a result, even if enhancement in heat transfer is observed, the demanded pumping power rises compared to the base fluid. This is due to a considerable increasement in dynamic viscosity that may end in an unfavorable energy balance. There exist diverse methods to describe the energy performance of liquids in a particular device (Sahiti et al. 2006). A criterion based on the general energy approach is the PEC calculated according to Eq. (11). This criterion is explained as ratio the net rate of useful heat gain of the HTF to the demanded pumping power (Ferrouillat et al. 2011; Roy et al. 2012).

$$PEC = \frac{\dot{m}C_p\left(T_{fo} - T_{fi}\right)}{\dot{V}\Delta P} \tag{11}$$

The next indicator is the overall efficiency, which alters the demanded pumping power parameter into primary energy and subsequently this amount of energy is deducted from the net rate of useful heat gain (Hasanpour et al. 2014; Wirz et al. 2014).

$$\eta_{ovr} = \frac{\dot{Q}_u - \frac{\dot{W}_p}{\eta_{el}}}{A_a I_{eff}} \tag{12}$$

The electrical efficiency is usually 33%.

Results and discussion

Uncertainty analysis

To accomplish a prosperous experiment, the analysis of the uncertainty is needed to measure the accuracy of the measurement. The parameters calculated in the present study could get divided into two categories. The first category is directly measured with laboratory instruments such as VFR, radiant heat flux, temperature, etc. The second category involves dependent parameters such as TE, Reynolds number, friction factor and demanded pumping power. The proposed method of uncertainty in heat transfer parameters is Kline and MCclintock method, which can be estimated using the root-sum-square method of every single separate inputs. The general form of this method is as follows (Sabatelli et al. 2002).

$$R = f\left(X_1, X_2, \ldots, X_N\right) \tag{13}$$

$$U_{C,X}(R) = \left\{ \sum_{i=I}^{N} \left(\frac{\delta R}{\delta X_i} U_{X_i} \right)^2 \right\}^{0.5} \tag{14}$$

where $U_{C,X}(R)$ and U_{X_i} indicate the uncertainty of the parameter R and the independent variable X_i, respectively. N in this relation is the number of independent variables. With the help of certain mathematical calculations, the relative uncertainty of TE is extracted according to Eq. (3) as follows.

$$\frac{U\eta_{th}}{\eta_{th}} = [(\frac{\delta\dot{V}}{\dot{V}})^2 + (\frac{\delta\rho_f}{\rho_f})^2 + (\frac{\delta C_p}{C_p})^2 + (\frac{\delta A_a}{A_a})^2 + (\frac{\delta I_{eff}}{I_{eff}})^2 + (\frac{\delta(T_{fo}-T_{fi})}{T_{fo}-T_{fi}})^2]^{0.5}$$
$$\frac{\delta(T_{fo}-T_{fi})}{T_{fo}-T_{fi}} \le \left[(\frac{\delta T_{fo}}{T_{fo}})^2 + (\frac{\delta T_{fi}}{T_{fi}})^2\right]^{0.5} = 1.01\% \tag{15}$$

By ignoring variation of A_a, ρ_f and C_p, the relative uncertainties of the other parameters measured are as follows.

$$\frac{\delta\dot{V}}{\dot{V}} \le 1.8\%, \frac{\delta I_{eff}}{I_{eff}} \le 2.5\% \tag{16}$$

$$\frac{\delta f}{f} = [(\frac{2\delta u}{u})^2 + (\frac{\delta\rho}{\rho})^2 + (\frac{\delta l}{l})^2 + (\frac{\delta D_H}{D_H})^2 + (\frac{\delta p}{p})^2]^{0.5} \tag{17}$$

Therefore, after the process of calculating the uncertainty of other important measured parameters, the maximum uncertainty is presented in Table 5. According to the engineering application of the conducted tests, these numbers are in an acceptable range.

Thermo-physical properties of the examined NF

For the purpose of representing the effect of suspension of the NP on the base fluid, the thermophysical properties of the NF are investigated in the first step. In this research, the thermal conductivity of NFs has been measured with the help of KD2 Pro device besides with KS1 sensor. Also, the dynamic viscosity of the NF is measured using the Brookfield DV1 Prime with UL Adapter and LAUDA RA8 temperature bath at the studied temperatures. It should be noted that due to the slight difference between the theoretical relationships of density and SHC with experiment values, these two parameters have been calculated using a single-phase model and mixing theory. This matter is also common in past research. The single-phase method is based on calculating the thermo-physical properties of NF based on the volumetric fraction of NPs. The NP

Table 5 Uncertainty of measured parameters

Parameter	Symbol	Uncertainty
Thermal efficiency	η_{th}	3.2%
Overall efficiency	η_{ovr}	3.7%
Friction factor	f_{Exp}	3.6%
Nusselt number	Nu	3%
Reynolds number	Re	3.5%
Pumping power	$\dot{W}_p$	2.08%
Performance evaluation criterion	PEC	2.25%

is symbolized with (np) while the NF and the base fluid are symbolized with (nf) and (bf), respectively.

$$\phi = \frac{V_{np}}{V_{nf}} = \frac{V_{np}}{V_{bf} + V_{np}} \tag{18}$$

The density of the NF could be evaluated utilizing the following formula (Loni et al. 2016; Saedodin et al. 2021).

$$\rho_{nf} = \frac{m_{nf}}{V_{nf}} = (1 - \phi)\rho_{bf} + \phi\rho_{np} \tag{19}$$

The SHC is modeled based on the reference analysis (Khanafer and Vafai 2018; Rashidi et al. 2018). This model is a function of the product of NF density multiplied by SHC, which is a role of the properties of NPs and the base fluid.

$$C_{p,nf} = \frac{\phi\left(\rho C_p\right)_{np} + (1-\phi)\left(\rho C_p\right)_{bf}}{\rho_{nf}} = \frac{\phi\left(\rho C_p\right)_{np}}{\rho_{nf}} + \frac{(1-\phi)\left(\rho C_p\right)_{bf}}{\rho_{nf}} \tag{20}$$

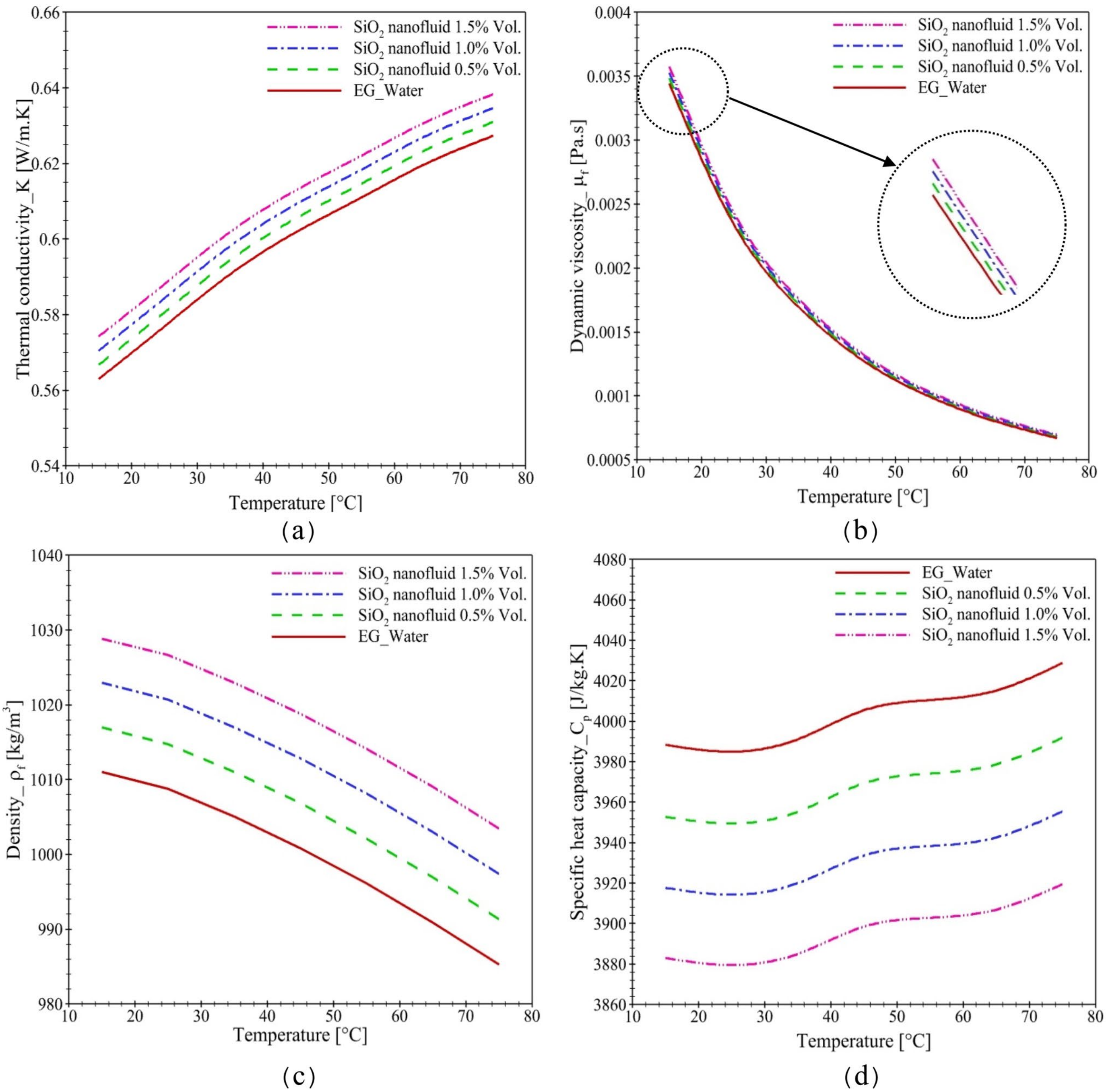

Fig. 7 Thermo-physical properties of NF versus different temperatures and volumetric fractions

Figure 7 displays the thermal conductivity, dynamic viscosity, density and SHC, respectively. The thermal conductivity of HTFs increased due to adding NPs into base fluid. Figure 7a shows that the value of enhancement in thermal conductivity of NF has about 0.62%, 1.24% and 1.86% than the base fluid in volumetric fraction of 0.5%, 1% and 1.5%, respectively. In addition, it is obvious that with increasing fluid temperature, thermal conductivity has an increasing rate. The pattern of increase in thermal conductivity can be discussed following the theory of Brownian motion. At higher temperatures the collision between particles rises as it leads to an enhancement in Brownian diffusion, which enhances the thermal conductivity. Also, NPs in the base fluid increase the thermal conductivity by decreasing the thickness of the thermal boundary layer, which rises the convection heat transfer. Brownian motion, shear action and spatial gradient in viscosity and distribution non-uniform conductivity in addition to the migration of NPs in the base fluid are the roots of the increase in NF thermal conductivity (Ding & Wen 2005).

The dynamic viscosity of the HTFs also plays an significant role in the performance of the solar collectors. Figure 7b represents that NF in volume fraction of 0.5%, 1% and 1.5% has about 1.27%, 2.57% and 3.89% higher dynamic viscosity compared to the EG-water. Furthermore, the dynamic viscosity decreases with increasing fluid temperature and this phenomenon is also reported by previous studies (Azmi et al. 2016). The dynamic viscosity of NFs rises due to the enhancement of internal shear stress and then increasing the volumetric fraction of NPs has a greater effect on this shear stress (Jabbari et al. 2017). The intermolecular interactions between particles are reduced at low temperatures. At higher temperatures, molecules obtain higher kinetic energy, which facilitates increased fluid motion and decreases dynamic viscosity (X. Li et al. 2015a, b). According to Newtonian fluid theory, shear stress and shear rate are directly related and dynamic viscosity remains constant. In this research, NFs at various volumetric fractions showed non-Newtonian behavior because the dynamic viscosity decreases with increasing shear stress at any given individual temperature.

To study density behavior, the density of the EG-water and NFs with various volumetric fractions in the temperature range of 15 to 75 °C has been calculated according to Eq. (19) and its data are shown in Fig. 7c. As shown in the figure, density enhanced with an increase in volumetric fractions of NFs (Nabati Shoghl et al. 2016) and decreases with an increase in temperature (Vajjha and Das 2009). The density of the NFs is higher than that of the base fluid. The minimum and maximum increase of density of the NFs are 0.60% and 1.82%. The data obtained from the SHC of the NF according to the Eq. (20) in all volumetric fractions are shown in Fig. 7d. There is a good relationship between SHC and thermal conductivity, especially with thermal diffusivity as NFs can diffuse heat much better than base fluid. Increasing volumetric fraction of NFs reduces the SHC of NFs due to increased thermal diffusivity of NFs (Sekhar et al. 2013). According to Fig. 7d, the SHC of the NF is less than the base fluid and the average value of the reduction in SHC of the NF is between 0.89 and 2.67%.While with increasing fluid temperature, the SHC increases. At this stage, it is useful to note that the values of thermal conductivity, density, and SHC of the NF are almost between the NPs and the values of the base fluid. These observations fully justify the results obtained from the studied NF, which convey higher thermal conductivity and density compared to the base fluid. Nevertheless, lower SHC than the base fluid is also observed. The dynamic viscosity of the NF is higher than the base fluid because the presence of NPs provides more resistance in fluid flow.

Thermal performance analysis of the CPC collector

The highest motivation for researchers to use nanofluids (instead of common fluids) is their improved thermal properties. Convective heat transfer and thermal efficiency are two important factors that are needed to be increased to give a better thermal performance in CPC collector. SiO_2/EG-water NF with 0.5%, 1%, and 1.5% volumetric fraction was used in the CPC collector as the HTF to assess the influence of different VFRs from 1 to 2.5 Lit/min. At first, to achive a greater level of understanding the impact of NF on the TP of the CPC collector, a smooth three-dimensional plot is drawn in Fig. 8. This diagram shows the simultaneous impact of VFR and volumetric fraction of NF on TE. As it is seen in the figure, the improvement of the TE of the NF compared to the base fluid is quite clear. TE also increases with increase in volumetric fraction and VFR of NF. As the VFR increases, the Reynolds number increases, thereby increasing the Brownian motion. The force generated from the collision of particles and molecules of the HTF induces the Brownian motion of the particles and this affects the heat conduction significantly

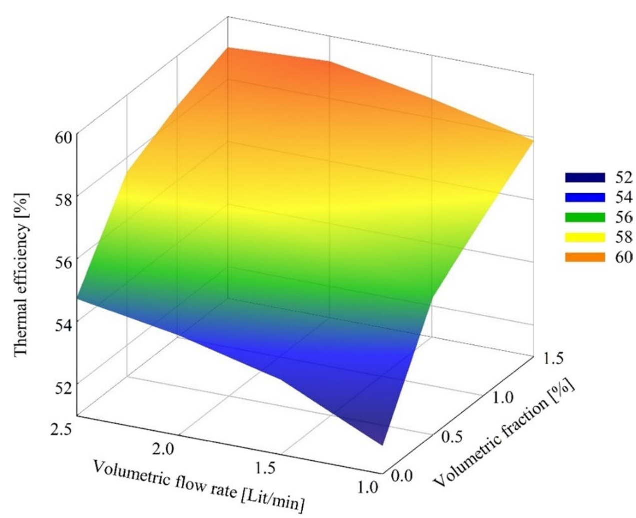

Fig. 8 The three-dimensional plot of TE versus volumetric fraction and VFR of NF

(Kleinstreuer & Xu 2016). NPs collide with the absorber tube wall with the properties of Brownian motion and dispersion, absorb heat, and go back to the mainly liquid part, which is good for heat transfer. Accordingly, the increase in the VFR of the fluid augments the contact of particles with the heat surface and this increases the heat transfer coefficient (Zeinali Heris et al. 2011). This behavior may be related to the change of collector TE with HTFs. Since less energy is dissipated at the VFR of 2.5 Lit/min for NF at volumetric fraction 1.5%, the highest TE (59.02%) is related to this VFR.

Figure 9 shows the effect of volumetric fraction on the characteristics of TE curves for different VFRs. Although the curve variations for base fluid and NFs are similar, but TE is significantly higher when NFs are used. By rising the concentration of NPs from 0.5 to 1.5%, the TE increases by approximately 5 to 11.6% when the reduced temperature is near 0. By increasing the reduced temperature factor, the impact of NF on the TP of the collector is greater and the difference in TE between the NFs and EG-water increases. Although the thermal conductivity of SiO_2 NPs is equal to 1.4 W/m.K, which is less than the

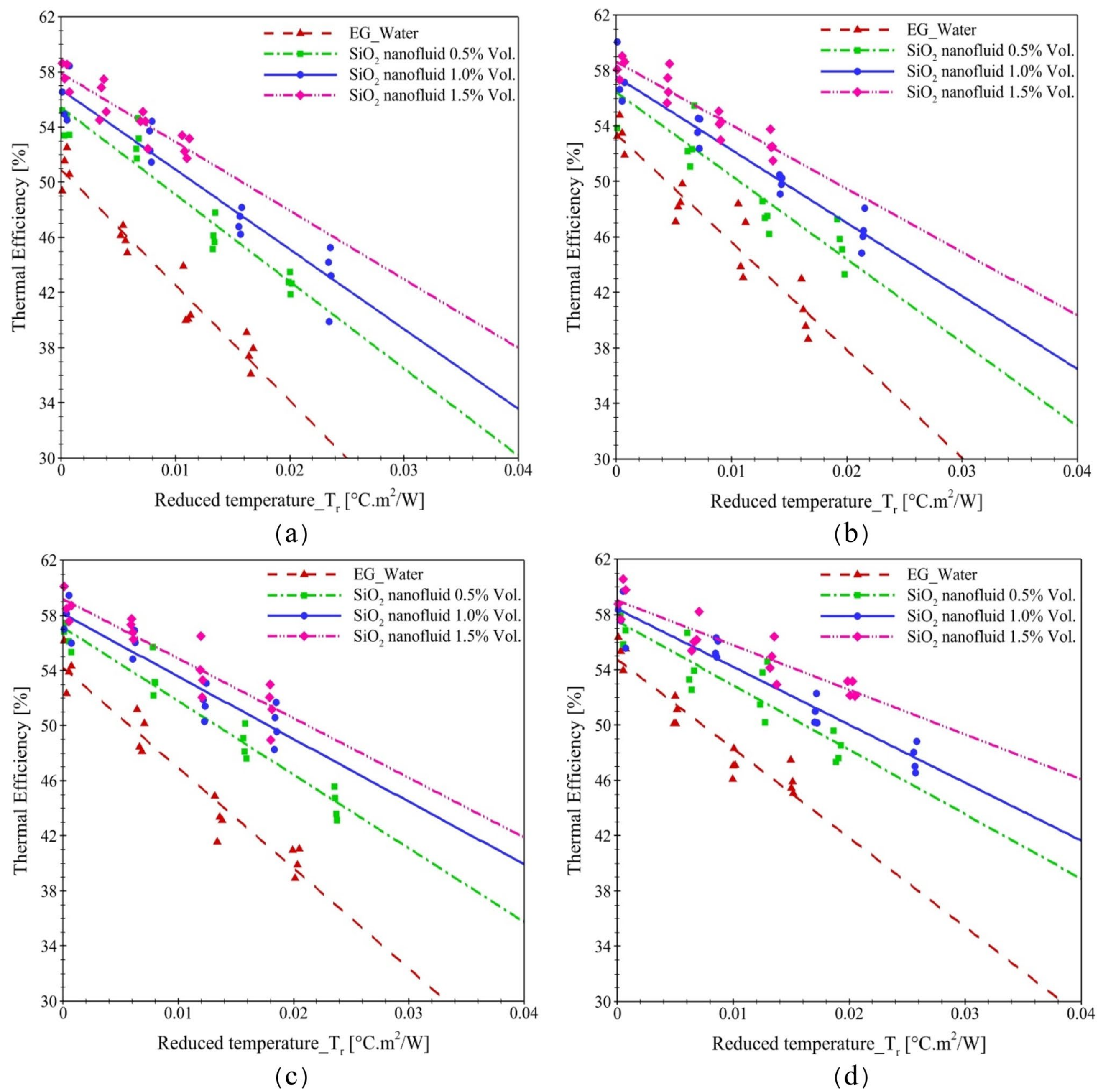

Fig. 9 Characteristic curves of CPC collector in various volumetric fraction and VFRs of (**a**) 1.0 *Lit/min*, (**b**) 1.5 *Lit/min*, (**c**) 2.0 *Lit/min*, and (**d**) 2.5 *Lit/min*

other NPs (Hasanpour et al. 2014; Mahian et al. 2017), the rate of increasement in TE of the CPC collector is significant. It is worth noting that the thermal conductivity of NFs is not the only key parameter that improves heat transfer and at the same time affects the TP of the collector. This improvement could be affected with various factors. NFs have a smaller SHC than the base fluid and its amount reduces with rising the volumetric fraction. Therefore, the use of NPs causes the outlet temperature of HTF to be higher. According to the definition of TE equation (Eq. (3)), when the increasement in outlet temperature of HTF overcomes the decrease in SHC of HTF, it can lead to the improvement of TE. Another parameter affecting heat transfer is the change in thickness of the thermal boundary layer, which can be analyzed by knowing the distribution of the temperature of operating HTF near the wall of the absorber tube. The heat transfer coefficient is written as follows (Bejan 2004).

$$h = \frac{-K_f \left(\frac{\partial T}{\partial r} \right)_{r=R}}{T_S - T_{fave}} \tag{21}$$

Utilizing scale analysis of δ_T, the heat transfer coefficient could be obtained as follows (Bejan 2004).

$$h \sim \frac{K_f \left(\frac{\Delta T}{\delta_T} \right)}{\Delta T} \sim \frac{k_f}{\delta_T} \tag{22}$$

From a microscopic point of view, Brownian motion of NPs and their re-arrangement due to nonuniform shear rate in the absorber tube can decrease the thickness of the boundary layer (Alim et al. 2013). Therefore, reducing the thickness of the thermal boundary layer in the NF flow plays an important role in improving the TP and compensating for its lack of thermal conductivity. On the other hand, deposition of NPs on the inner surfaces of absorber tube makes an artificial layer which increased the surface wettability, capillary effect, TE of the collector, while it decreased thermal resistance by decreasing the bubble formation rate at the solid–liquid interface (Rezaeian et al. 2021).

Figure 10 displays the impacts of VFR on the characteristics of the curve of the TE for different volumetric fraction of NF. The changes in the TE of the CPC collector for four VFRs of the base fluid as the HTF compared to the reduced temperature parameters is shown in Fig. 10a. It can be recognized that the TE of the CPC collector is minimal at the VFR of 1 Lit/min and rises are seen in TE (from 51.9 to 54.75%) as VFR is enhanced to 2.5 Lit/min. Figure 10b to d shows the TE of SiO_2/EG-water NF in volumetric fractions of 0.5%, 1%, and 1.5% with different VFRs (1, 1.5, 2 and 2.5 Lit/min), respectively. According to these figures, when the VFR of the HTF enhances, the TE of the collector improves. Different factors influence the TE of a CPC collector. VFR, inlet temperature of HTF, and coefficient of heat transfer are effective internal factors of the collector, and solar radiation and ambient temperature are external effective factors of the collector. One of the internal main factors is the VFR of the HTF. At a low VFR, the HTF had a greater chance to transfer heat, so that the difference between the inlet and outlet temperatures of the collector was enhanced. Table 6 represents this relationship. As it is clear in this table, as the VFR and fluid speed were enhanced, the difference between the inlet and outlet temperature of the collector has decreased. According to Eq. (1), more volume of fluid gained energy with the increase in VFR, which leads to a decrease in heat loss. Also, the multiplication product of the VFR in the temperature rise is so that the energy absorption rate increases even when the VFR is increased; hence, the TE of the collector is improved. The lower the temperature difference between the inlet fluid of the collector and the surrounding environment, in other words, the smaller the reduced temperature, the lower the heat losses and the higher the TE of the collector will be. Therefore, the increase in ambient temperature enhances the TE of a collector and finally increases the outlet temperature of the collector (Zhang et al. 2006). This is clearly seen in Figs. 9 and 10. As shown in Fig. 9a to d, the maximum TE of CPC collector for base fluid, NF with volumetric fraction of 0.5%, NF with volumetric fraction of 1% and NF with volumetric fraction of 1.5% as heat transfer fluid was increased to 54.75%, 57.53%, 58.4%, and 59.02%, respectively, when the VFR of was enhanced to 2.5 Lit/min. Therefore, the ideal VFR can be set to 2.5 Lit/min. One of the significant results in Table 6 is the increase in the outlet temperature of the HTF from the collector with the increase in volumetric fraction. Addition of SiO_2 NPs to the base fluid leads to the internal surface temperature of absorber tube reduces. Therefore, more solar radiation is absorbed by the NF-absorber tube and converted to thermal energy. In addition, it was found that increasing the volumetric fraction of NPs causes an improvement in the effective thermal conductivity and increases the heat transfer coefficient. This event increases the outlet temperature of the HTF and enhancment the TE.

The properties extracted from the TE curves for base fluid and NFs are presented in Table 7. It is observed that NFs with higher volumetric fraction can increase the $F_R\eta_0$ and also it reduces the F_RU_L. According to this table, at VFR of 2.5 Lit/min, using NF with a volumetric fraction of 0.5%, 1% and 1.5%, respectively, the TE is increased by 2.7%, 3.65%, and 4.27%. Due to the removed energy parameter (F_RU_L) is lower with SiO_2 than with base fluid. In the CPC collector with NF, the movement of NPs, such as Brownian motion and other irregular motions, increases the collision of the fluid flow with the wall of the absorber tube, and as a result, the coefficient of convection heat transfer increases. The increase of the net rate of useful heat gain leads to a decrease in average temperature of the absorber tube surface, which means less heat loss. Finally, TE increases and less energy is lost. Also, at a constant VFR, with the increase in volumetric fraction of NF, the amount of absorbed energy parameter increases and as a result, the TE increases. Because the fraction of

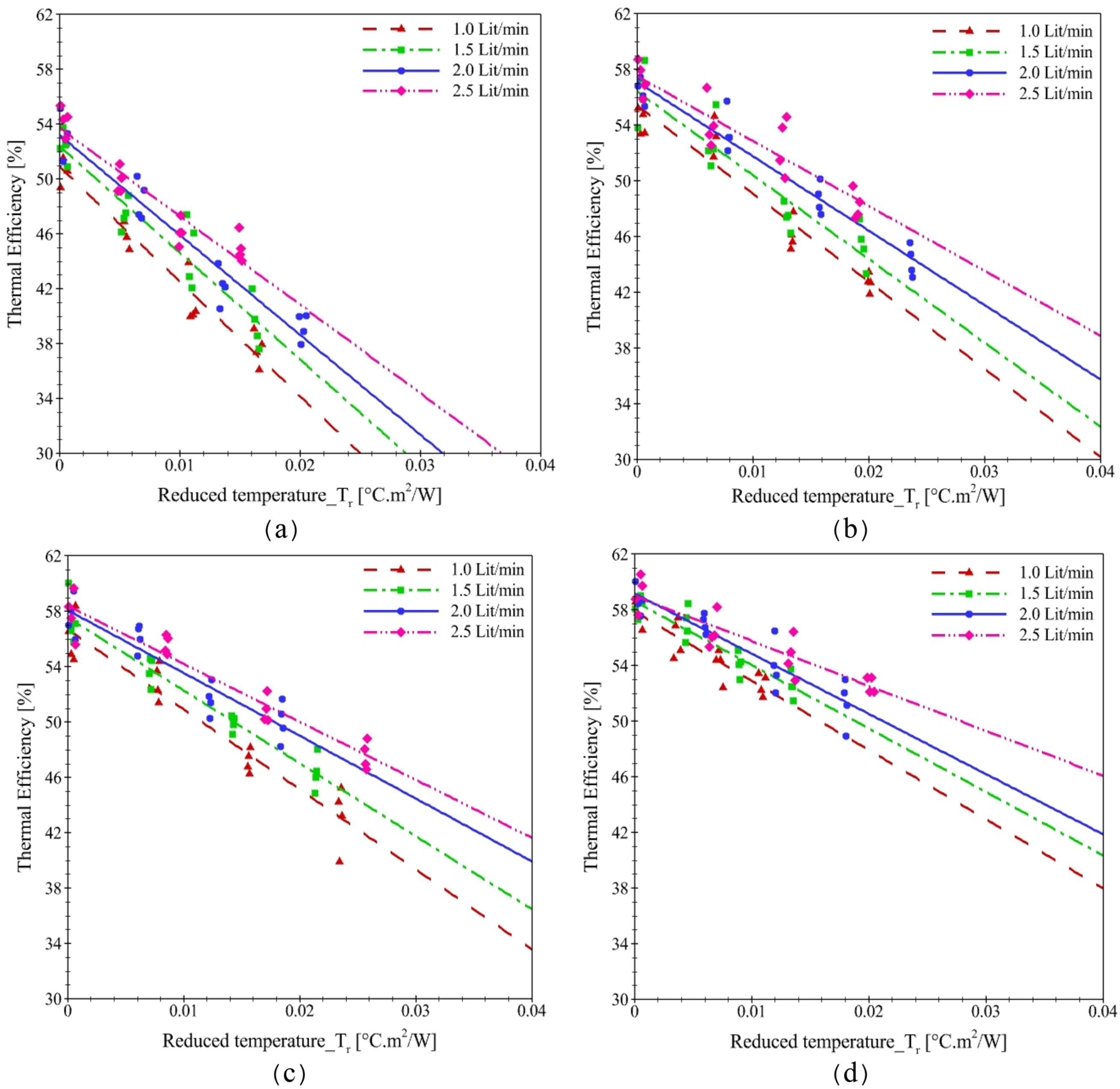

Fig. 10 Characteristic curves of the CPC collector in various VFRs and volumetric fraction of (**a**) 0%, (**b**) 0.5%, (**c**) 1.0%, and (**d**) 1.5%

Table 6 The inlet and outlet temperature difference of the HTF at the ambient temperature 25°C

	$\Delta T = T_{fo} - T_{fi}$			
Volumetric flow rate ($\frac{Lit}{Min}$)	$\phi = 0.0\%$	$\phi = 0.5\%$	$\phi = 1.0\%$	$\phi = 1.5\%$
1.0	2.73	3.08	3.18	3.22
1.5	1.93	2.06	2.12	2.19
2.0	1.40	1.58	1.64	1.66
2.5	1.12	1.26	1.29	1.34

incoming radiation absorbed by the fluid depends on its attenuation coefficient. When NF is used as the HTF, its damping coefficient increases by increasing the volumetric component of NF. At low volumetric fraction, little radiation is absorbed by the NF and the rest hits the wall and is reflected. As the volumetric fraction increases, the amount of radiation absorbed by the NF increases and as a result the temperature of the outlet NF increases, which leads to higher TE. But the TE increases to a certain extent with the increase of volumetric fraction of NF, and then it does not change much, in other words, it behaves independently of the volumetric fraction.

Table 7 Absorbed energy parameter $\left(F_R\eta_0\right)$ and removed energy parameter $\left(F_RU_L\right)$ of the CPC collector for HTF

Nanofluids concentration	$F_R\eta_0$				F_RU_L			
	1 Lit/min	1.5 Lit/min	2 Lit/min	2.5 Lit/min	2.5 Lit/min	2 Lit/min	1.5 Lit/min	1 Lit/min
0% (EG-Water)	0.5190	0.5340	0.5420	0.5475	10.965	12.376	13.209	14.212
0.5% vol	0.5541	0.5643	0.5712	0.5753	7.922	9.078	10.217	10.727
1.0% vol	0.5670	0.5755	0.5810	0.5840	7.123	7.718	8.959	9.8260
1.5% vol	0.5789	0.5862	0.5919	0.5902	5.491	7.344	7.769	8.4660

The reason for this is that by increasing the volumetric fraction of NF, the convective heat transfer coefficient of the HTF increases and consequently, the value of the overall heat transfer coefficient is increased, which leads to an increase in thermal dissipation due to the difference between the HTF temperature and the ambient temperature.

A comparison of Table 7 and Fig. 9 shows that the TE increases with the increase in VFR, regardless of the type of HTF (base fluid or NF). This phenomenon can be attributed to the fact that although the HTF experiences a higher temperature rise at lower VFRs than at higher VFRs because the HTF remains in the absorber tube for a longer period of time, the lower VFRs entail more heat losses by convection and radiance. Therefore, when the flow rate is increased, since the NF is exposed to sunlight for a shorter period of time, the heat loss to the outer environment is lessened, and as a result, the TE of the CPC collector is enhanced with the increase in the VFR. In general, the results of the experiments show that the TE of the CPC collector is improved with the increase in VFR.

To better compare the characteristics of the curve of TE, the changes of the $F_R\eta_0$ and the F_RU_L are shown in Fig. 11 in terms of volumetric fraction and VFR. Figure 11a shows the relative effect of base fluid and NF for each VFR on the maximum TE of the CPC collector. Absorbed energy parameter rises with enhancing both volumetric fraction of NFs and VFR. The maximal growth of the $F_R\eta_0$ occurs in the concentration range from 0.5 to 1.5% at VFR of 2.5 Lit/min. According to this diagram, the highest increment in the $F_R\eta_0$ compared to the lower concentration occurs in the volumetric fraction of 0.5%. It is followed by the highest increasement in TE compared to the base fluid in the same volumetric fraction. Also, it is clear from this figure that using SiO_2/EG-Water NF is more effective at lower VFRs than base fluid. Figure 11b exhibits that the use of NFs reduces the F_RU_L. This means that heat loss in the NF flow is reduced compared to the base fluid. In addition, the higher volumetric fraction has the lower the heat loss. Reducing the F_RU_L by increasing the VFR at each concentration is the other outstanding feature of this figure. As the HTF passes through the absorber tube rapidly, the heat loss in the collector is reduced and, consequently, the F_RU_L is decreased.

The Nu is utilized as a dimensionless parameter to determine the TP of the NF flow of the CPC collector. The

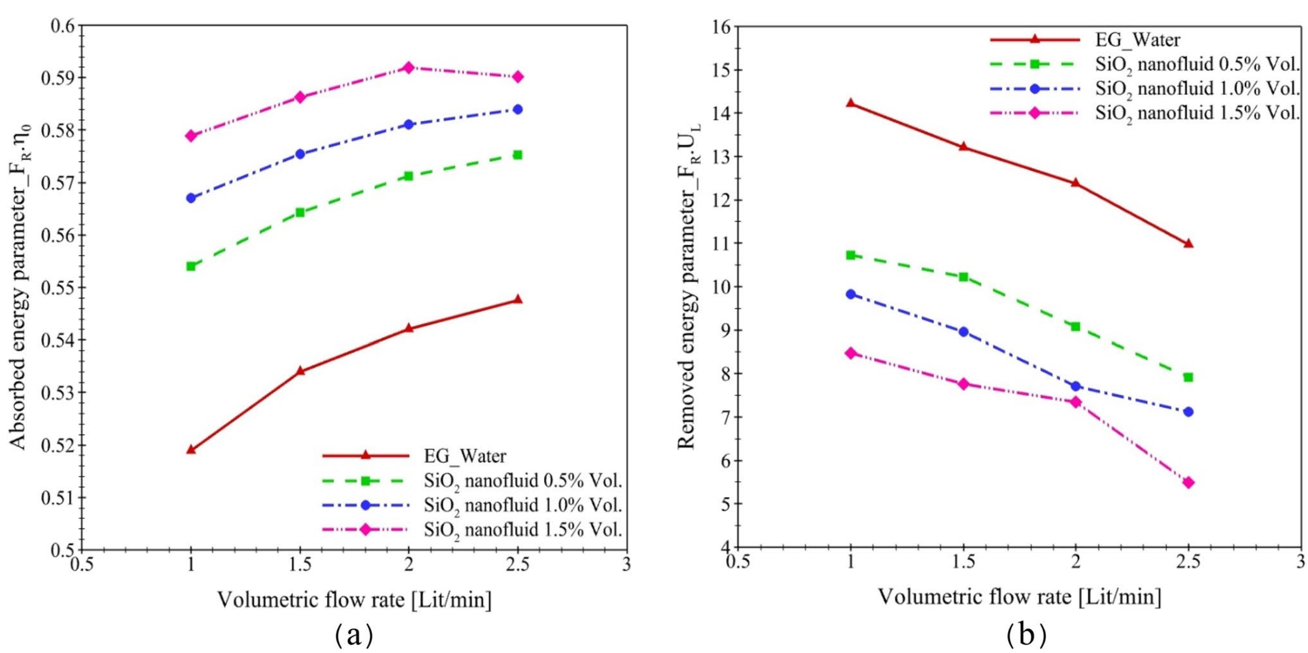

Fig. 11 Variations of the (**a**) $F_R\eta_0$, (**b**) F_RU_L versus volumetric fraction in different VFR

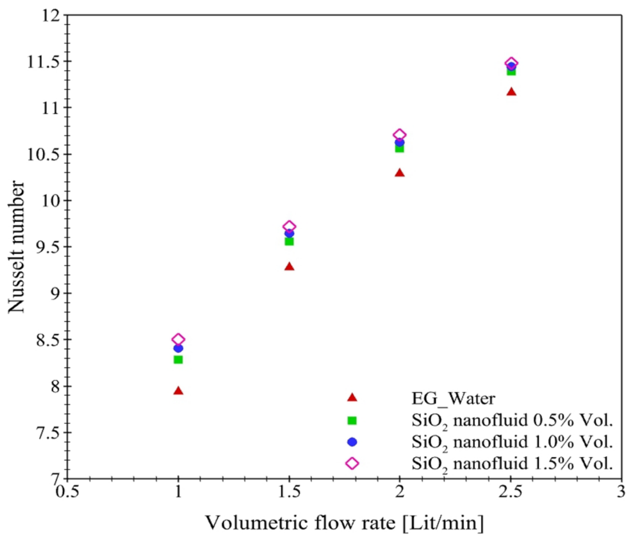

Fig. 12 Changes of the Nu number versus the VFR

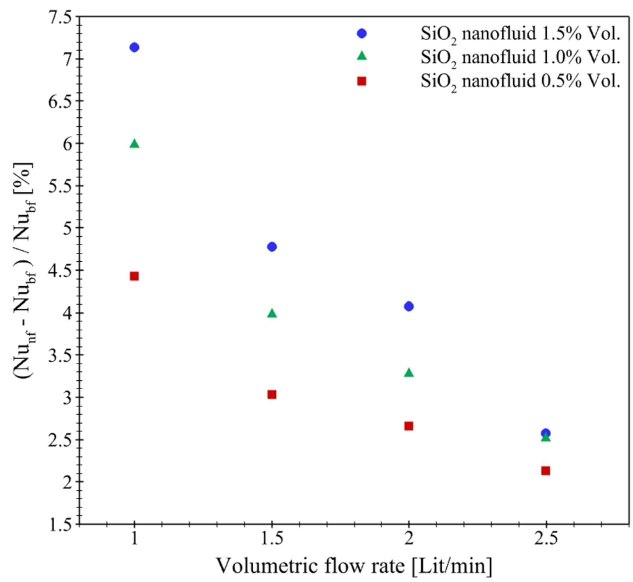

Fig. 13 Relative increment of the Nu due to NF

Nu evaluated at the temperature of the inlet fluid is near the environment temperature. The use of NFs, as HTFs, increases the thermal conductivity inside the fluid and therefore the heat transfer coefficient and Nu increases. This fact is given in Fig. 12. The enhancement is ranged from 2.36 up to 7.31%, which seems to be an adequate result. The outcomes represent that by using the NF, the Nu is improved. The Nu also rises with increasing volumetric fraction.

Figure 13 demonstrates the relative increment of the Nu in the CPC collector. This parameter is defined as $Nu_{nf} - Nu_{bf}/Nu_{bf}$. According to the results, the relative increment of the Nu has a reducing trend with rising the VFR. Also, at each volumetric fraction of the NF, this parameter is more significant at the smaller VFR.

In the final part of this section, it is beneficial to state that the utilization of NF leads to an enhancement in heat transfer coefficient. Higher values of heat transfer coefficient facilitate heat transfer from the absorber tube to the fluid. Therefore, the temperature levels of the absorber tube decrease because of the effective cooling of the NF flow. In practice, when the heat transfer coefficient is higher, the $T_s - T_{fave}$ difference is smaller for producing the same useful heat rate. Thermal radiation is the main cause of heat loss in the absorber tube which is proportional to the fourth power of the temperature of absorber tube surface (T_s^4). Therefore, lower temperature of the absorber tube surface leads to lower heat loss of thermal radiation and it increases the TE of the CPC collector. This mechanism explains the reason why the use of NF is beneficial for solar thermal system.

Hydraulic analysis of the CPC collector

The utilization of the NF to improve the TP of the CPC collector is associated with an increasement in pressure drop at flow direction. Therefore, it is necessary to assess the pressure drop in order to have efficient use of this ability without significantly increasing the pumping power for industrial purposes. Also, the friction factor is used both in the calculation of pressure drop and heat transfer of fluids; it is due to the reason that the determination of pressure drop is an important parameter for CPC collector performance. Shah's equation for friction factor (dimensionless pressure parameter) for the hydrodynamically developing length X_h ($Re \lesssim 2300, X_h \approx 0.05DRe_D$) is used to confirm the experimental results of base fluid in absorber tube as follows (Shah and London 1978):

$$f = \frac{\Delta P}{\frac{L}{2r_{a_i}}\left(\frac{1}{2}\rho_f u_m^2\right)} = \frac{2r_{a_i}}{L}\left[13.74\left(\frac{x}{2r_{a_i}Re_D}\right)^{0.5} + \frac{1.25 + 64\left(\frac{x}{2r_{a_i}Re_D}\right) - 13.74\left(\frac{x}{2r_{a_i}Re_D}\right)^{0.5}}{1 + 0.0002\left(\frac{x}{2r_{a_i}Re_D}\right)^{-2}}\right] \quad (23)$$

The values calculated according to Eq. (23) for friction factor are presented in Fig. 14 and compared to the empirical outcomes. The maximum increment in friction factor of 6.8% occurs in the volumetric fraction of 1.5%. The results represent that the use of NF in all volumetric fractions does not lead to a significant increasement in friction factor and as expected, the amount of friction factor decreased with increasing the VFR.

An important mechanical aspect of pressure drop is pumping power which is directly related to it. The impact of NF on pumping power at different VFRs is presented in Fig. 15. As can be seen, by increasing the VFR, the pumping power was increased. According to this figure, at low VFR, the pumping power of NFs is approximately equal with the base fluid. On the other hand, by increasing the VFR, the amount of pumping power in NFs is higher than the base fluid. The maximum increasement in pumping power when using NFs at VFR of 2.5 Lit/min is equal to 3.58%. The NF has a higher dynamic viscosity and it causes a greater pressure drop, which results in an extra penalization in the fluid flow enhancement. The pressure drop rises the demand for pumping power for fluid circulation.

Also, increasing heat transfer along with enhancing pumping power has been provided by addition of NPs to the base fluid. Thus, heat transfer and pumping power results do not present the concluding result separately. To assess this situation, appropriate criteria should be employed. So as to simultaneously assess the rise of pumping power and heat transfer, overall efficiency and PEC are being utilized. Figure 16 represents the overall efficiency diagram at the VFR of 2.5 Lit/min, which has the highest pumping power. This diagram

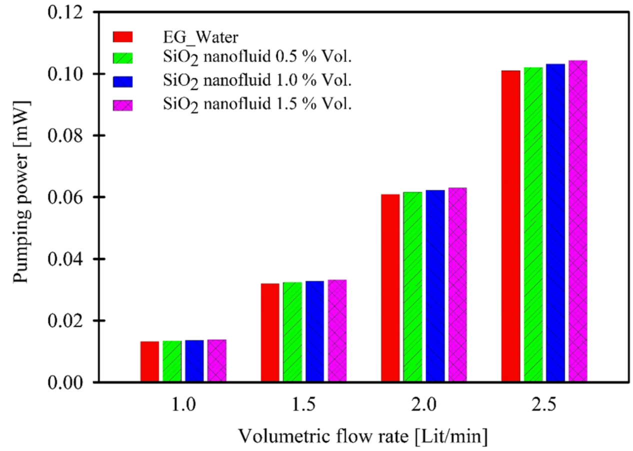

Fig. 15 Changes of the pumping power versus the VFR

shows that the utilization of NFs in the CPC collector despite the increment of pumping power, improves overall efficiency.

The last criterion studied is PEC, the changes of which are evaluated against the VFR in Fig. 17. For three volumetric fractions (0.5%, 1%, and 1.5%), the PEC value of the NFs is higher than that of the base fluid. The PEC of NF has a downward trend against the VFR. In addition, PEC is almost close to each other with different volumetric fractions. The minimum and maximum increase in PEC is 1.61% and 14.41%. As observed, PEC has a larger value in smaller volumetric fractions and in 0.5% volumetric fraction the PEC value is higher than the other two volumetric fractions. Finally, by determining the two criteria of overall efficiency and PEC, it can be stated that SiO_2/EG-water NFs are more suitable working fluids in comparison with base

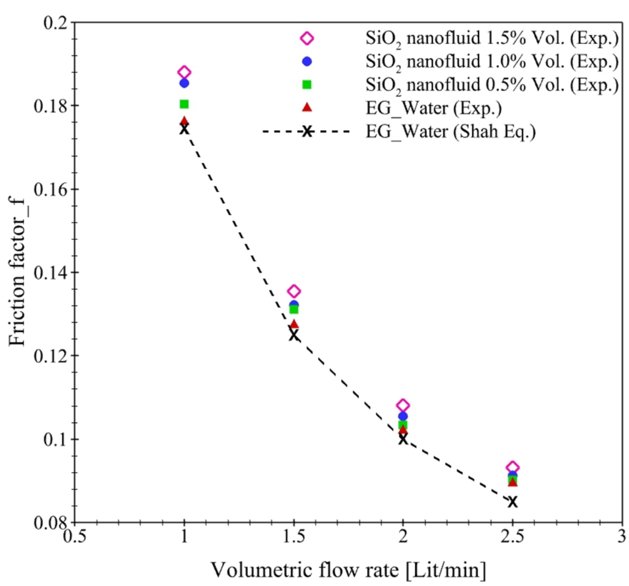

Fig. 14 Changes of the friction factor (dimensionless pressure) versus VFR (Line for Shah's equation and without line for experimental results)

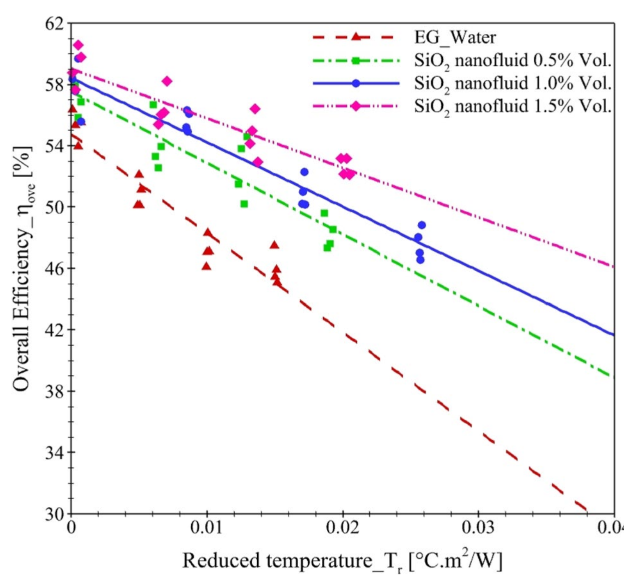

Fig. 16 Changes of the overall efficiency in VFR of 2.5 Lit/min

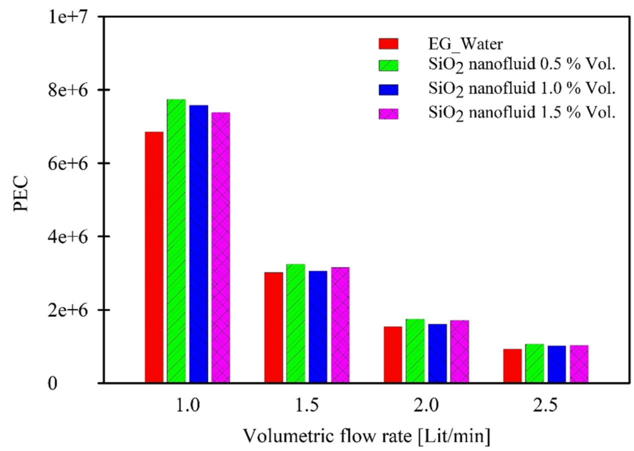

Fig. 17 Changes of the PEC versus the VFR

fluid in the CPC collector. It appears that the enhancement of pumping power is less important compared to increase of heat transfer coefficient and this fact makes the increase of pumping power not a limitation in the use of NFs.

Conclusion

In this paper, the TP of a CPC collector with NF containing silica NPs was experimentally studied. Experiments were carried out according to ASHRAE standard 93–2010 (RA2014) at variation environmental conditions, four VFRs and three different volumetric fractions. The main objective was placed on comparing variation HTFs in terms of the TE of collector and evaluation criteria for NF effects on collector performance. Some of the highlights of the present research are stated as follows:

- Compared to the base fluid, the use of SiO_2/EG-water NF in the CPC collector had higher TE and less heat loss at all reduced temperatures.
- The outcomes showed that when the reduced temperature parameter was close to 0, rising the volumetric fraction of NF from 0.5 to 1.5% leads to an increment in TE between 5 and 11.6% at different VFR.
- The characteristics of the curve of collector performance displayed that the impact of using NPs on increasing the TE of the CPC collector was greater in higher values of reduced temperature.
- As the VFR increased, the TE of the CPC collector for the base fluid and NFs enhanced. However, this rate of increase in TE for NFs was greater than for the base fluid.
- At lower VFR, the effect of NP addition on the TE gains became more pronounced. At VFR of 1 Lit/min, when SiO_2 NPs were added to the EG-water, the increase in TE were 6.73%, 9.24%, and 11.60% for volumetric fractions of 0.5%, 1%, and 1.5%, respectively.
- Experimental data represented that the $F_R\eta_0$ decreased with rising the VFR of NF.
- PEC had a reducing trend with increasing VFR. The largest increase in volumetric fraction of 0.5% occurred compared to the EG-water.
- The maximal increase in friction factor and demanded pumping power was 6.8% and 3.58%, respectively.
- Analysis of the outcomes showed that SiO_2 NPs, despite lower thermal conductivity compared to other conventional NPs, had great potential to improve the TP of the CPC collector.

This experimental study has provided a more accurate and comprehensive insight into the utilization of an oxide NF in the CPC collector. It could be perceived that the use of oxide NFs in volumetric fractions less than 1.5% in the CPC collector increased the TE by imposing a slight pumping power. Finally, improving TP and rising the TE of the CPC collector bring about a higher, output temperature both in domestic and industrial applications.

Author contribution O. Khaledi and S. H. Rostamian conceived of the presented idea; O. Khaledi and S. H. Rostamian carried out the experiment and collected the data; O. Khaledi wrote the manuscript with support from S. H. Rostamian and S. Saedodin. All the authors discussed the results and contributed to the final manuscript. S. Saedodin supervised the project; all the authors read and approved the final manuscript.

Funding The authors would like to acknowledge the financial support of Semnan University for this project under grant number 139908101001.

Data availability The data will be made available on request.

Declarations

Competing interests The authors declare no competing interests.

References

Akbarzadeh S, Valipour MS (2018) Heat transfer enhancement in parabolic trough collectors: a comprehensive review. Renew Sustain Energy Rev 92:198–218. https://doi.org/10.1016/j.rser.2018.04.093
Alim MA, Abdin Z, Saidur R, Hepbasli A, Khairul MA, Rahim NA (2013) Analyses of entropy generation and pressure drop for a conventional flat plate solar collector using different types of metal oxide nanofluids. Energy and Buildings 66:289–296. https://doi.org/10.1016/j.enbuild.2013.07.027
Ashrae S (2014) S standard methods of testing to determine the thermal performance of solar collectors - Catalog - UW-Madison Libraries. https://search.library.wisc.edu/catalog/999821471802121

Azmi WH, Hamid KA, Usri NA, Mamat R, Mohamad MS (2016) Heat transfer and friction factor of water and ethylene glycol mixture based TiO2 and Al2O3 nanofluids under turbulent flow. Int Commun Heat Mass Transfer 76:24–32

Bejan A (2004) Convection heat transfer, Third Edition. John Wiley & Sons Inc, New York, pp 96–167. https://books.google.com/books

Bellos E, Tzivanidis C, Said Z (2020) A systematic parametric thermal analysis of nanofluid-based parabolic trough solar collectors. Sustain Energy Technol Assess 39:100714. https://doi.org/10.1016/j.seta.2020.100714

Brunold S, Frey R, Frei U (1994) Comparison of three different collectors for process heat applications. Optic Mater Technol Energy Efficiency Solar Energy Conversion XIII 2255:107–118. https://doi.org/10.1117/12.185361

Çengel YA, Cimbala JM (2013) Fluid mechanics: fundamentals and applications, Third Edition. In McGraw-Hill (Vol. 53, Issue 9). https://books.google.com/books

Dadashi Z, Mahmoudi A, Rashidi S (2022) Capacity and strategies of energy production from renewable sources in Arab countries until 2030: a review from renewable energy potentials to environmental issues. Environ Sci Pollut Res. https://doi.org/10.1007/S11356-022-20544-Z

Ding Y, Wen D (2005) Particle migration in a flow of nanoparticle suspensions. Powder Technol 149(2–3):84–92. https://doi.org/10.1016/j.powtec.2004.11.012

Duffie JA, Beckman WA, McGowan J (1985) Solar engineering of thermal processes. Am J Phys 53(4):382–382. https://doi.org/10.1119/1.14178

Esfanjani P, Jahangiri S, Heidarian A, Valipour MS, Rashidi S (2022) A review on solar-powered cooling systems coupled with parabolic dish collector and linear Fresnel reflector. Environ Sci Pollut Res 29(28):42616–42646. https://doi.org/10.1007/S11356-022-19993-3

Farhana K, Kadirgama K, Mohammed HA, Ramasamy D, Samykano M, Saidur R (2021) Analysis of efficiency enhancement of flat plate solar collector using crystal nano-cellulose (CNC) nanofluids. Sustainable Energy Technol Assess 45. https://doi.org/10.1016/j.seta.2021.101049

Fernández-García A, Zarza E, Valenzuela L, Pérez M (2010) Parabolic-trough solar collectors and their applications. Renew Sustain Energy Rev 14(7):1695–1721. https://doi.org/10.1016/j.rser.2010.03.012

Ferrouillat S, Bontemps A, Ribeiro JP, Gruss JA, Soriano O (2011) Hydraulic and heat transfer study of SiO2/water nanofluids in horizontal tubes with imposed wall temperature boundary conditions. Int J Heat Fluid Flow 32(2):424–439. https://doi.org/10.1016/j.ijheatfluidflow.2011.01.003

Hasanpour A, Farhadi M, Sedighi K (2014) A review study on twisted tape inserts on turbulent flow heat exchangers: the overall enhancement ratio criteria. Int Commun Heat Mass Transfer 55:53–62. https://doi.org/10.1016/j.icheatmasstransfer.2014.04.008

Izadi M, Shahmardan MM, Behzadmehr A (2013) Richardson number ratio effect on laminar mixed convection of a nanofluid flow in an annulus. Int J Comput Methods Eng Sci Mech 14(4):304–316. https://doi.org/10.1080/15502287.2012.749313

Izadi M, Behzadmehr A, Shahmardan MM (2014) Effects of discrete source-sink arrangements on mixed convection in a square cavity filled by nanofluid. Korean J Chem Eng 31(1):12–19. https://doi.org/10.1007/s11814-013-0176-7

Izadi M, El Haj Assad M (2021) Use of nanofluids in solar energy systems. In Design and Performance Optimization of Renewable Energy Systems (pp. 221–250). Elsevier. https://doi.org/10.1016/B978-0-12-821602-6.00017-1

Jabbari F, Rajabpour A, Saedodin S (2017) Thermal conductivity and viscosity of nanofluids: a review of recent molecular dynamics studies. In Chemical Engineering Science (Vol. 174, pp. 67–81). https://doi.org/10.1016/j.ces.2017.08.034

Jouybari HJ, Saedodin S, Zamzamian A, Nimvari ME, Wongwises S (2017) Effects of porous material and nanoparticles on the thermal performance of a flat plate solar collector: an experimental study. Renewable Energy 114:1407–1418. https://doi.org/10.1016/j.renene.2017.07.008

Kalogirou SA (2014) Solar energy engineering: processes and systems: Second Edition. In Solar Energy Engineering: Processes and Systems: Second Edition. https://doi.org/10.1016/C2011-0-07038-2

Khaledi O, Saedodin S, Rostamian SH (2022b) Energy, hydraulic and exergy analysis of a compound parabolic concentrator using hybrid nanofluid: an experimental study. Int Commun Heat Mass Transfer 136:106181. https://doi.org/10.1016/j.icheatmasstransfer.2022.106181

Khaledi, O., Saedodin, S., & Rostamian, S. H. (2022a). Optimization of the nonlinear model of neural network training in predicting thermal efficiency of solar concentrator with simulated annealing algorithm. Int J Nonlinear Anal Applic 2008–6822. https://doi.org/10.22075/IJNAA.2021.22254.2341

Khanafer K, Vafai K (2018) A critical synthesis of thermophysical characteristics of nanofluids. Nanotechnol Energy 279–332. https://doi.org/10.1201/9781315163574-12/CRITICAL-SYNTHESIS-

Kharabati S, Saedodin S, Rostamian SH (2021) Experimental investigation of thermal and rheological behavior of silica/ soybean oil nano lubricant in low-temperature performance of internal combustion engine. Energy Sources A: Recov, Util Environ Effects. https://doi.org/10.1080/15567036.2021.1897193

Kleinstreuer C, Xu Z (2016) Mathematical modeling and computer simulations of nanofluid flow with applications to cooling and lubrication. Fluids 1(2):16. https://doi.org/10.3390/fluids1020016

Korres D, Bellos E, Tzivanidis C (2019) Investigation of a nanofluid-based compound parabolic trough solar collector under laminar flow conditions. Appl Therm Eng 149:366–376. https://doi.org/10.1016/j.applthermaleng.2018.12.077

Li X, Zou C, Wang T, Lei X (2015b) Rheological behavior of ethylene glycol-based SiC nanofluids. Int J Heat Mass Transf 84:925–930. https://doi.org/10.1016/j.ijheatmasstransfer.2015.01.104

Li Q, Zheng C, Mesgari S, Hewakuruppu YL, Hjerrild N, Crisostomo F, Morrison K, Woffenden A, Rosengarten G, Scott JA, Taylor RA (2015a) Experimental investigation of a nanofluid absorber employed in a low-profile, concentrated solar thermal collector. 9668, 323–335. https://doi.org/10.1117/12.2202513

Loni R, Kasaeian AB, Mahian O, Sahin AZ (2016) Thermodynamic analysis of an organic rankine cycle using a tubular solar cavity receiver. Energy Convers Manage 127:494–503. https://doi.org/10.1016/j.enconman.2016.09.007

Mahbubul IM, Khan MMA, Ibrahim NI, Ali HM, Al-Sulaiman FA, Saidur R (2018) Carbon nanotube nanofluid in enhancing the efficiency of evacuated tube solar collector. Renew Energy 121:36–44. https://doi.org/10.1016/j.renene.2018.01.006

Mahian O, Kianifar A, Kalogirou SA, Pop I, Wongwises S (2013) A review of the applications of nanofluids in solar energy. Int J Heat Mass Transf 57(2):582–594. https://doi.org/10.1016/j.ijheatmasstransfer.2012.10.037

Mahian O, Kianifar A, Heris SZ, Wen D, Sahin AZ, Wongwises S (2017) Nanofluids effects on the evaporation rate in a solar still equipped with a heat exchanger. Nano Energy 36:134–155. https://doi.org/10.1016/j.nanoen.2017.04.025

Minea AA (2017) Hybrid nanofluids based on Al2O3, TiO2 and SiO2: numerical evaluation of different approaches. Int J Heat Mass Transf 104:852–860. https://doi.org/10.1016/j.ijheatmasstransfer.2016.09.012

Nabati Shoghl S, Jamali J, KeshavarzMoraveji M (2016) Electrical conductivity, viscosity, and density of different nanofluids: an experimental study. Exp Thermal Fluid Sci 74:339–346. https://doi.org/10.1016/j.expthermflusci.2016.01.004

Naveenkumar R, Ravichandran M, Stalin B, Ghosh A, Karthick A, Aswin LSRL, Priyanka SSH, Kumar SP, Kumar SK (2021) Comprehensive review on various parameters that influence the performance of parabolic trough collector. Environ

Sci Pollut Res 28(18):22310–22333. https://doi.org/10.1007/S11356-021-13439-Y
Okonkwo EC, Wole-Osho I, Kavaz D, Abid M, Al-Ansari T (2020) Thermodynamic evaluation and optimization of a flat plate collector operating with alumina and iron mono and hybrid nanofluids. Sustain Energy Technol Assess 37:100636. https://doi.org/10.1016/j.seta.2020.100636
Panahi R, Khanjanpour MH, Javadi AA, Akrami M, Rahnama M, Ameri M (2019) Analysis of the thermal efficiency of a compound parabolic integrated collector storage solar water heater in Kerman Iran. Sustain Energy Technol Assess 36:100564. https://doi.org/10.1016/j.seta.2019.100564
Rashidi S, Mahian O, Languri EM (2018) Applications of nanofluids in condensing and evaporating systems: a review. J Therm Anal Calorim 131(3):2027–2039. https://doi.org/10.1007/S10973-017-6773-7
Rashidi S, Hormozi F, Karimi N, Ahmed W (2021) Applications of nanofluids in thermal energy transport. In Emerging Nanotechnologies for Renewable Energy (pp. 345–368). Elsevier. https://doi.org/10.1016/B978-0-12-821346-9.00018-3
Rezaeian M, ShafieyDehaj M, ZamaniMohiabadi M, Salarmofrad M, Shamsi S (2021) Experimental investigation into a parabolic solar collector with direct flow evacuated tube. Appl Therm Eng 189:116608. https://doi.org/10.1016/j.applthermaleng.2021.116608
Rostamian SH, Saedodin S, Asgari SA, Salarian AH (2022) Effect of C60-SiO2 hybrid nanoparticles on thermophysical and tribological properties of a multigrade engine oil: an experimental study. J Therm Anal Calorim 147(1):155–167. https://doi.org/10.1007/s10973-020-10323-8
Roy G, Gherasim I, Nadeau F, Poitras G, Nguyen CT (2012) Heat transfer performance and hydrodynamic behavior of turbulent nanofluid radial flows. Int J Therm Sci 58:120–129. https://doi.org/10.1016/j.ijthermalsci.2012.03.009
Sabatelli V, Marano D, Braccio G, Sharma VK (2002) Efficiency test of solar collectors: uncertainty in the estimation of regression parameters and sensitivity analysis. Energy Convers Manage 43(17):2287–2295. https://doi.org/10.1016/S0196-8904(01)00180-7
Sadeghi G, Nazari S, Ameri M, Shama F (2020) Energy and exergy evaluation of the evacuated tube solar collector using Cu2O/water nanofluid utilizing ANN methods. Sustain Energy Technol Assess 37:100578. https://doi.org/10.1016/j.seta.2019.100578
Sadeghiazad MM, Yahou S (2018) Numerical investigation on effect of nanofluid on compound parabolic solar collector performance- Part 2: type and volume fraction of nano particle. Prog Sol Energy Eng Syst 2:1–4
Saedodin S, Rostamian SH, Zaboli M (2021) Hydrothermal analysis and optimization of heat transfer and pressure drop characteristics of different nanofluids in a circular tube with turbulator. Eur Phys J Plus, 136(7). https://doi.org/10.1140/epjp/s13360-021-01678-4
Sahiti N, Lemouedda A, Stojkovic D, Durst F, Franz E (2006) Performance comparison of pin fin in-duct flow arrays with various pin cross-sections. Appl Therm Eng 26(11–12):1176–1192. https://doi.org/10.1016/j.applthermaleng.2005.10.042
Sajjadi H (2021) Natural convection heat transfer in a porous cavity with sinusoidal temperature distribution using Cu/water nanofluid: double MRT lattice Boltzmann method. Commun Comput Phys 29(1):292–318. https://doi.org/10.4208/cicp.OA-2020-0001
SalavatiMeibodi S, Kianifar A, Niazmand H, Mahian O, Wongwises S (2015) Experimental investigation on the thermal efficiency and performance characteristics of a flat plate solar collector using SiO2/EG-water nanofluids. Int Commun Heat Mass Transfer 65:71–75. https://doi.org/10.1016/j.icheatmasstransfer.2015.02.011
Sekhar Y (2013) Study of viscosity and specific heat capacity characteristics of water-based Al2O3 nanofluids at low particle concentrations. Taylor & Francis 10(2):86–102. https://doi.org/10.1080/17458080.2013.796595.
ShafieyDehaj M, Ahmadi M, ZamaniMohiabadi M (2020) Assessment of a heat pipe solar collector with nanofluids. Environ Sci Pollut Res 28(5):5316–5331. https://doi.org/10.1007/S11356-020-10797-X
Shah R, London A (1978) Laminar flow forced convection in ducts, Supplement 1 to advances in heat transfer. Academic Press
Sharafeldin MA, Gróf G (2018) Evacuated tube solar collector performance using CeO2/water nanofluid. J Clean Prod 185:347–356. https://doi.org/10.1016/j.jclepro.2018.03.054
Shehzad SA, Mabood F, Rauf A, Izadi M, Abbasi FM (2021) Rheological features of non-Newtonian nanofluids flows induced by stretchable rotating disk. Phys Scr 96(3):035210. https://doi.org/10.1088/1402-4896/abd652
Tahani M, Vakili M, Khosrojerdi S (2016) Experimental evaluation and ANN modeling of thermal conductivity of graphene oxide nanoplatelets/deionized water nanofluid. Int Commun Heat Mass Transfer 76:358–365. https://doi.org/10.1016/j.icheatmasstransfer.2016.06.003
Unar IN, Maitlo G, Abbasi SA, Abro M, Qureshi RF, Memon SA, Hussain T, Mangi KH (2021) Modeling and simulation of solar flat plate collector for energy recovery at varying regional coordinates. Environ Sci Pollut Res 29(3):4748–4761. https://doi.org/10.1007/S11356-021-15869-0
Ustaoglu A, Alptekin M, Okajima J, Maruyama S (2016) Evaluation of uniformity of solar illumination on the receiver of compound parabolic concentrator (CPC). Sol Energy 132:150–164. https://doi.org/10.1016/j.solener.2016.03.014
Vajjha RS, Das DK (2009) Experimental determination of thermal conductivity of three nanofluids and development of new correlations. Int J Heat Mass Transf 52(21–22):4675–4682. https://doi.org/10.1016/j.ijheatmasstransfer.2009.06.027
Wirz M, Petit J, Haselbacher A, Steinfeld A (2014) Potential improvements in the optical and thermal efficiencies of parabolic trough concentrators. Sol Energy 107:398–414. https://doi.org/10.1016/j.solener.2014.05.002
Xiong Q, Altnji S, Tayebi T, Izadi M, Hajjar A, Sundén B, Li LKB (2021a) A comprehensive review on the application of hybrid nanofluids in solar energy collectors. Sustainable Energy Technol Assess 47. https://doi.org/10.1016/j.seta.2021.101341
Xiong Q, Hajjar A, Alshuraiaan B, Izadi M, Altnji S, Shehzad SA (2021b) State-of-the-art review of nanofluids in solar collectors: a review based on the type of the dispersed nanoparticles. J Clean Prod 310(2):127528. https://doi.org/10.1016/j.jclepro.2021.127528
Yan S-R, Izadi M, Sheremet MA, Pop I, Oztop HF, Afrand M (2020) Inclined Lorentz force impact on convective-radiative heat exchange of micropolar nanofluid inside a porous enclosure with tilted elliptical heater. Int Commun Heat Mass Transfer 117:104762. https://doi.org/10.1016/j.icheatmasstransfer.2020.104762
ZeinaliHeris S, Noie SH, Talaii E, Sargolzaei J (2011) Numerical investigation of Al2O3/water nanofluid laminar convective heat transfer through triangular ducts. Nanoscale Res Lett 6(1):179. https://doi.org/10.1186/1556-276X-6-179
Zhang X, Gu H, Fujii M (2006) Effective thermal conductivity and thermal diffusivity of nanofluids containing spherical and cylindrical nanoparticles. J Appl Phys 100(4):044325. https://doi.org/10.1063/1.2259789